Neuro-Oncology

20(4), 567–575, 2017 | doi:10.1093/neuonc/nox159 | Advance Access date 24 August 2017

Early posttreatment assessment of MRI perfusion biomarkers can predict long-term response of lung cancer brain metastases to stereotactic radiosurgery

Neil K. Taunk, Jung Hun Oh, Amita Shukla-Dave, Kathryn Beal, Behroze Vachha, Andrei Holodny, and Vaios Hatzoglou

Department of Radiation Oncology (N.K.T., K.B.), Neuroradiology Service, Department of Radiology (B.V., A.H., V.H.), and Department of Medical Physics (J.H.O., A.S.D.), Memorial Sloan Kettering Cancer Center, New York, New York

Corresponding Author: Vaios Hatzoglou, MD, Department of Radiology, Memorial Sloan Kettering Cancer Center, 1275 York Avenue, New York, NY 10065 (hatzoglV@mskcc.org).

Abstract

Background. Imaging criteria to evaluate the response of brain metastases to stereotactic radiosurgery (SRS) in the early posttreatment period remains a crucial unmet need. The aim of this study is to correlate early (within 12 wk) posttreatment perfusion MRI changes with long-term outcomes after treatment of lung cancer brain metastases with SRS.

Methods. Pre- and posttreatment perfusion MRI scans were obtained in patients treated with SRS for intact non–small cell lung cancer brain metastases. Time-dependent leakage (K^{trans}), blood plasma volume (Vp), and extracellular extravascular volume (Ve) were calculated for each lesion. Patients were followed longitudinally with serial MRI until death, progression, or intervention (whole brain radiation or surgery).

Results. We included 53 lesions treated with SRS from 41 total patients. Median follow-up after treatment was 11 months. Actuarial local control at one year was 85%. Univariate analysis demonstrated a significant difference (P = 0.032) in posttreatment K^{trans} SD between patients with progressive disease (mean = 0.0317) and without progressive disease (mean = 0.0219). A posttreatment K^{trans} SD cutoff value of 0.017 was highly sensitive (89%) for predicting progressive disease and no progressive disease. Early posttreatment volume change was not associated with outcome (P = 0.941).

Conclusion. Posttreatment K^{trans} SD may be used as an early posttreatment imaging biomarker to help predict long-term response of lung cancer brain metastases to SRS. This can help identify patients who will ultimately fail SRS and allow for timelier adjustment in treatment approach. These data should be prospectively validated in larger patient cohorts and other histologies.

Key words

brain metastases | MRI | perfusion MRI | radiation therapy | stereotactic radiosurgery

Brain metastases (BMs) are the most common intracranial malignancy in adults, such that up to 40% of brain tumors are metastatic in origin and approximately 200 000 new cases are diagnosed each year. Cancers of the lung, in particular, have a high propensity to spread to the brain.[1] For these patients, prognosis is generally guarded given that BMs often correspond with increasing systemic disease or resistance to current therapy.[2,3] Currently, radiation therapy (RT) is the most commonly used modality to treat BMs, for either palliative or curative intent.[4–6] For patients with one or several lesions, stereotactic radiosurgery (SRS) in a single session is often used in place of whole brain RT (WBRT), yielding >80%–90% durable local control.[7] Given improvements in systemic therapy, particularly targeted therapies or those with CNS penetration, certain subsets of patients are able to live longer. Unfortunately, many patients with brain metastases treated with SRS fail to respond. Developing a non-invasive imaging biomarker to

Importance of the study

SRS can eradicate or control brain metastasis but is unsuccessful in up to 20% of patients at 1 year after therapy. Tumor volume change on initial post-SRS MRI is unreliable for predicting long-term outcome. Our study demonstrates that post-radiation therapy (RT) K^{trans} SD may be utilized as a noninvasive imaging biomarker of early therapeutic efficacy. The ability to rapidly identify unresponsive lesions allows for timelier consideration of alternative therapies and may help optimize patient management.

Unlike prior studies evaluating brain metastases after RT, we focused on non–small cell lung cancer treated only with SRS. This allows control of confounding variables such as different tumor histologies and the effect of non-ablative radiation treatments such as whole brain RT. Additionally, the majority of patients were followed until death, giving a more complete understanding of the long-term utility of perfusion MRI biomarkers. These data should be prospectively validated in larger patient cohorts.

optimize patient selection and identify nonresponders is a critical unmet need, as patients may require early treatment intensification if they are determined to be at high risk for failure.

MRI is the gold standard for initial evaluation of BMs and monitoring of treatment response after brain radiation. MRI provides superior sensitivity and delineation compared with other methods, including contrast-enhanced CT.[8] Advanced MRI techniques, including contrast-enhanced perfusion, spectroscopy, and diffusion tensor imaging, can provide significant functional information in addition to excellent anatomic information such as that provided by conventional MRI.[9] Dynamic-contrast enhanced (DCE) MR perfusion imaging (pMRI) is an advanced imaging technique that allows for quantitative assessment of tumor microvasculature by analyzing the distribution kinetics of an intravenously injected low-molecular-weight paramagnetic agent in the microvessels and extracellular extravascular space of tissue under review.[10] MR perfusion imaging allows for assessment of physiologic changes in the lesion and extraction of quantitative data for longitudinal tumor monitoring. These data can be characterized as non-invasive imaging biomarkers, and studies are beginning to emerge regarding their utility in monitoring treatment response.

A crucial issue in the management of BMs is how to best assess treatment response early after RT, particularly in the case of SRS. Treatment success is generally regarded as the absence of progression in the size of the lesion. Nearly one half of BMs after radiation may increase in size, and that increase in size may persist in up to 12% even at 15 months post-radiation.[11] The size increase is often transient and complicates management decisions, which are further confounded by histology of the lesion or concomitant systemic therapy. The reference standard in characterizing the nature of enlarging lesions is surgical resection, but this is not feasible or necessary in a patient population with advanced disease and asymptomatic lesion enlargement. Although several working groups have established criteria to provide some uniformity in assessing response, they do not address the functional changes in the tumor that would show a physiologic response to radiation.[12]

We hypothesize that early (within 12 wk) post-SRS quantitative analysis of perfusion imaging can predict whether or not lung cancer BMs will ultimately respond or fail treatment. These quantifiable data would in turn allow physicians to create a platform for personalization of RT by rapid identification of patients who are suitable for observation after RT or who may require treatment intensification.

Materials and Methods

Patients and Treatment

This study was performed at a tertiary cancer institution in accordance with the Health Insurance Portability and Accountability Act and with local institutional review board approval, including a waiver of informed consent. Patients were retrospectively identified from 2012 to 2015. During this time we established routine pMRI acquisition before and after SRS treatment. Patients who were included met the following criteria: histopathologic diagnosis of non–small cell lung cancer (NSCLC), treatment of an intact (nonresected) brain metastasis with SRS, pretreatment pMRI, and posttreatment pMRI within 12 weeks after treatment. Patients who received WBRT prior to SRS were excluded. Patients who did not have the treated lesion assessed with both pre- and posttreatment pMRI were also excluded. Patient data collected included patient age, histologic subtype, tridimensional lesion size, lesion location, SRS treatment dose (Gy), treatment dates, imaging dates, and any additional interventions (WBRT, surgery). Treatment was performed using single-fraction SRS alone with previously described techniques.[13] Molecular testing was performed on a biopsy of each patient's primary or a metastatic lesion. Primary tumors were genotyped with the Sequenom MassARRAY system analysis for common mutations in lung cancer, including epidermal growth factor receptor (EGFR), KRAS, BRAF, phosphatidylinositol-4,5-bisphosphate 3-kinase catalytic subunit alpha (PIK3CA), MEK1, NRAS, Akt1, and Erb-B2 receptor tyrosine kinase 2 (ERBB2)/human epidermal growth factor receptor 2 (HER2), as previously described.[14] Supplemental testing (PCR, fluorescence in situ hybridization) was performed to detect exon 19 and exon 20 deletions and anaplastic lymphoma kinase (ALK) rearrangements.

MR Perfusion Imaging Acquisition

Patients were scanned on 1.5T or 3T scanners (Signa Excite, HDx and Discovery 750, GE Healthcare) using an 8-channel head coil. Standard T1-weighted, T2-weighted,

diffusion-weighted, fluid-attenuated inversion recovery, susceptibility-weighted, and contrast T1-weighted images were acquired in multiple planes. Gadopentetate dimeglumine (Magnevist; Bayer HealthCare Pharmaceuticals) was power-injected via an intravenous catheter (18–21 gauge) at doses standardized by patient body weight (0.2 mL/kg body weight, maximum 20 mL) at 2–3 mL/s. High resolution 3D T1-weighted contrast-enhanced images in the axial plane with a slice thickness of 1 mm and no gaps between slices were routinely acquired for SRS planning and follow-up after therapy. T1-weighted DCE perfusion data were acquired using an axial 3D echo-spoiled gradient-echo sequence (repetition time [TR], 4–5 ms; echo time [TE], 1–2 ms; section thickness, 5 mm; flip angle, 25 degrees; field of view, 24 cm; matrix, 256 × 128). Ten phases were acquired pre-injection followed by another 30 phases during the dynamic injection of intravenous contrast. This was followed by a 40-mL saline flush. The time between phases (temporal resolution) was 5–6 seconds. Matching contrast T1-weighted (TR/TE, 600/8 ms; thickness, 5 mm; matrix, 256 × 224) spin-echo images were obtained. Ten to 12 slices were obtained for the DCE color maps and matching T1 postcontrast images to cover the volumes of the lesions. The native T1 was not measured and a fixed baseline value of 1000 ms was utilized.

Imaging Analysis

Data processing and analysis of pharmacokinetic variables were conducted using NordicICE version 2 (NordicNeuroLab). This applies a pharmacokinetic model of contrast uptake to the calculated signal intensity changes over time. Using a 2-compartment kinetic model, the contrast agent is presumed to be distributed in the blood plasma volume, leaking in a time-dependent manner into the interstitium. Preprocessing of pMRI included background noise removal and deconvolution with the arterial input function (AIF). A linear assumption was made between change in signal intensity and gadolinium concentration to convert the signal intensity curve to a concentration-time curve. The AIF was obtained from the middle cerebral artery independently for every patient. Curves showing an optimal relationship between AIF and the concentration-time curve were carefully selected. Time-dependent leakage (K^{trans}), blood plasma volume (Vp), and extracellular extravascular volume (Ve) were calculated using Toft's pharmacokinetic model analysis on a voxel-by-voxel basis.[15,16] All regions of interest (ROIs) were manually delineated by a trained operator on the matching axial T1 postcontrast scans. A board-certified attending neuroradiologist with 10 years of neuroimaging experience approved all ROIs. The edge of contrast enhancement on the T1 postcontrast scan dictated the borders of the lesions, including enhancing tumor tissue and cystic/necrotic changes, but not adjacent vessels. An average value was computed for metastases that spanned multiple axial slices. Histogram analysis was also performed on all voxels within the ROI.

Data Analysis

We analyzed 3 DCE-MRI metrics, including K^{trans}, Vp, and Ve. For each metric, we computed 3 submetrics, including mean, standard deviation (SD), and median, leading to a set of 9 features. The SD describes the width of the distribution of all voxels in a histogram analysis and is indicative of the heterogeneity of the tumor. We generated 3 sets of the 9 features: pre-RT, post-RT, and the change of values (denoted as Δ) between pre-RT and post-RT. In addition, we analyzed 3 clinical features, including pre-RT tumor volume, post-RT tumor volume, and RT dose, resulting in 30 features in total. For each imaging feature, an average value was computed across multiple slices on each lesion. Univariate analysis was performed using the Wilcoxon rank-sum test to find the degree of differences in these features between patients with and without progressive disease (PD). For features with *P*-values <0.1, principal component analysis followed by the Wilcoxon rank-sum test was conducted to investigate whether patients with PD are differentiated from patients without PD.

For clinical data, local control was assessed by the modified Response Assessment in Neuro-Oncology Brain Metastases (RANO-BM) criteria using conventional MRI, with additional information from surgical resection if performed after SRS.[12] The modification we made to standard RANO-BM criteria was to lower the minimum size limit of measurable disease to 5 mm. We chose to lower the limit because we routinely treat BMs measuring between 5 and 10 mm with SRS at our institution. Volumetric data were collected using standard tridimensional measurement (length × width × height/2). Local relapse-free survival was calculated from day of treatment to most recent imaging. Failure was determined by progressive disease defined by RANO-BM or surgical resection indicating viable tumor. All data were analyzed using GraphPad Prism version 7 and MatLab version R2014a.

Results

A total of 53 BMs were included for analysis, from 41 total patients (Table 1). Thirty-two patients had a solitary metastasis, 7 patients had 2 lesions, and 2 patients had more than 2 lesions. All lesions were treated with single-fraction SRS with median dose 21 Gy (range, 18–22 Gy). There were 35/41 (85%) patients with lung adenocarcinoma, 3/41 (7%) with poorly differentiated carcinoma, 2/41 (5%) with squamous cell carcinoma, and 1 with large cell carcinoma. Of the 53 included lesions, 19 were reimaged between 7 and 8 weeks, 16 by 10 weeks, and 18 by 12 weeks. Median follow-up after treatment was 11 months (range, 3.7–38.3 mo) and 73% of patients were followed until death. Actuarial local control at 1 year was 85% as determined by RANO-BM criteria or by pathologic determination if resected (Fig. 1). Rates of complete response (CR), partial response (PR), stable disease, and PD were 9%, 49%, 21%, and 21%, respectively. One patient required resection for a growing mass after SRS and was found to have viable tumor. Eight patients received WBRT after SRS for treatment of non-index metastases. Approximately 90% (48 of 53) of the BMs we evaluated met the RANO-BM size criteria for measurable disease. We included 5 lesions that were smaller, with none measuring below 5 mm. Of these, 3 demonstrated

Table 1 Patient characteristics

Characteristic		*N* (%)
Number	Patients	41
	Lesions	53
Sex	Male	21 (51.2)
	Female	20 (48.8)
Age, y	Median (range)	52 (36–71)
Histologic subtype (by patient)	Adenocarcinoma	35 (85.4)
	Squamous cell	3 (7.3)
	Large cell	1 (2.4)
	Poorly differentiated/ not otherwise specified	2 (4.9)
Mutation (by patient)	Wild type	15 (36.6)
	KRAS exon 2 G12c/D/V	11 (26.8)
	ALK rearranged	3 (7.3)
	ERBB2/HER2 exon 20 insertion	1 (2.4)
	EGFR exon 19 deletion	1 (2.4)
	KRAS exon 3 Q61H	1 (2.4)
	PIK3CA E542Q	1 (2.4)
	Not reported	8 (19.5)
Number of lesions	Single	29 (70.7)
	Multiple	12 (29.3)
Location	Supratentorial	46 (86.8)
	Infratentorial	7 (13.2)
Radiation dose	Median (range)	21 Gy (18–22)
Pre-RT tumor volume	Median (range)	450 mm^3 (40–3960)
Post-RT tumor volume	Median (range)	210 mm^3 (0–6075)

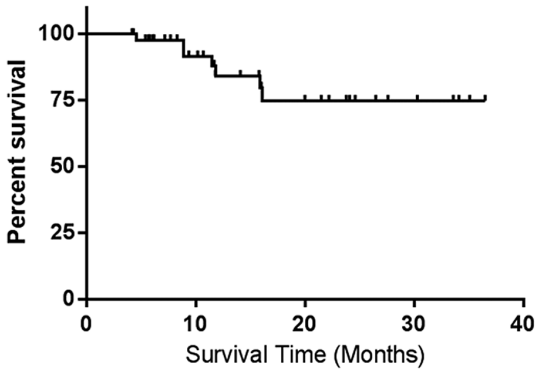

Fig. 1 Kaplan–Meier estimate of local control after SRS.

PD with increases in size of at least 3 mm: 2 increased by 8 mm and 1 lesion increased by 4 mm.

Representative anatomic and perfusion MR images before and after radiation treatment are shown in Fig. 2.

Univariate analysis using a Wilcoxon rank-sum test demonstrated a significant difference (P = 0.032) in post-RT K^{trans} SD between patients with PD (mean 0.0317) and without PD (mean 0.0219). This is summarized in Fig. 3. Using the Youden index, we determined that a post-RT K^{trans} SD cutoff value of 0.017 yields a balanced sensitivity (89%) and specificity (67%) for predicting PD and non-PD. Receiver operating characteristic analysis showed area under the curve = 0.73 for this value. Four features including post-RT K^{trans} mean, post-RT K^{trans} median, Δ K^{trans} SD, and Δ K^{trans} median showed a trend toward significance with $P < 0.1$ as shown in Table 2. Fig. 4 shows the distribution of patients for 2 principal components after principal component analysis using the 5 features. Principal components 1 and 2 correlated most strongly with post-RT K^{trans} SD and Δ K^{trans} median, respectively. It should be noted that patients with PD clustered on the right side. Fisher's exact test based on the boundary (seen as the vertical line of dots) showed that patients with PD are significantly differentiated from patients without PD (P = 0.0014).

Volume increase or decrease on the first follow-up scan was not significantly associated with long-term BM outcome defined by RANO-BM criteria (P = 0.9413). Of the 9 lesions that ultimately failed SRS, only 2 had increased in volume on the first posttreatment MRI. Post-RT K^{trans} SD correctly predicted long-term failure in both lesions using the cutoff value provided above. Seven lesions that ultimately failed SRS demonstrated an initial volume decrease. Post-RT K^{trans} SD correctly predicted treatment failure for 6 of 7 of these lesions.

No patients received systemic therapy concurrently with SRS. Our usual institutional practice is for patients to have a washout period of approximately 2 weeks before and after radiation for systemic therapy or 1 week before and after radiation for targeted systemic agents. There were 2 exceptions in our cohort: 1 patient received systemic therapy 2 days prior to SRS and another patient resumed therapy 5 days after SRS. Overall, there was a median 14 days between last systemic therapy prior to radiation and a median 13 days after radiation before resuming systemic therapy. There were 28/53 lesions (53%) that received systemic therapy prior to radiation and 40/53 lesions (76%) that received systemic therapy after radiation. The difference in lesion outcome (PD vs non-PD) between patients who received systemic therapy after SRS and those who did not was statistically insignificant (P = 0.33).

Forty-four percent (n = 18) of patients had some molecular aberration detected by Sequenom or supplemental methods, with the most common being in KRAS (exon 2 G12V/G12C/G12D, n = 11). There was no significant association between any pretreatment pMRI biomarker and presence or absence of a mutation. Supplemental analysis was performed on patients with KRAS mutations, as they formed our largest subgroup. Using the Wilcoxon rank-sum test we found that pretreatment Ve was significantly higher (P = 0.043) in BMs harboring KRAS mutations

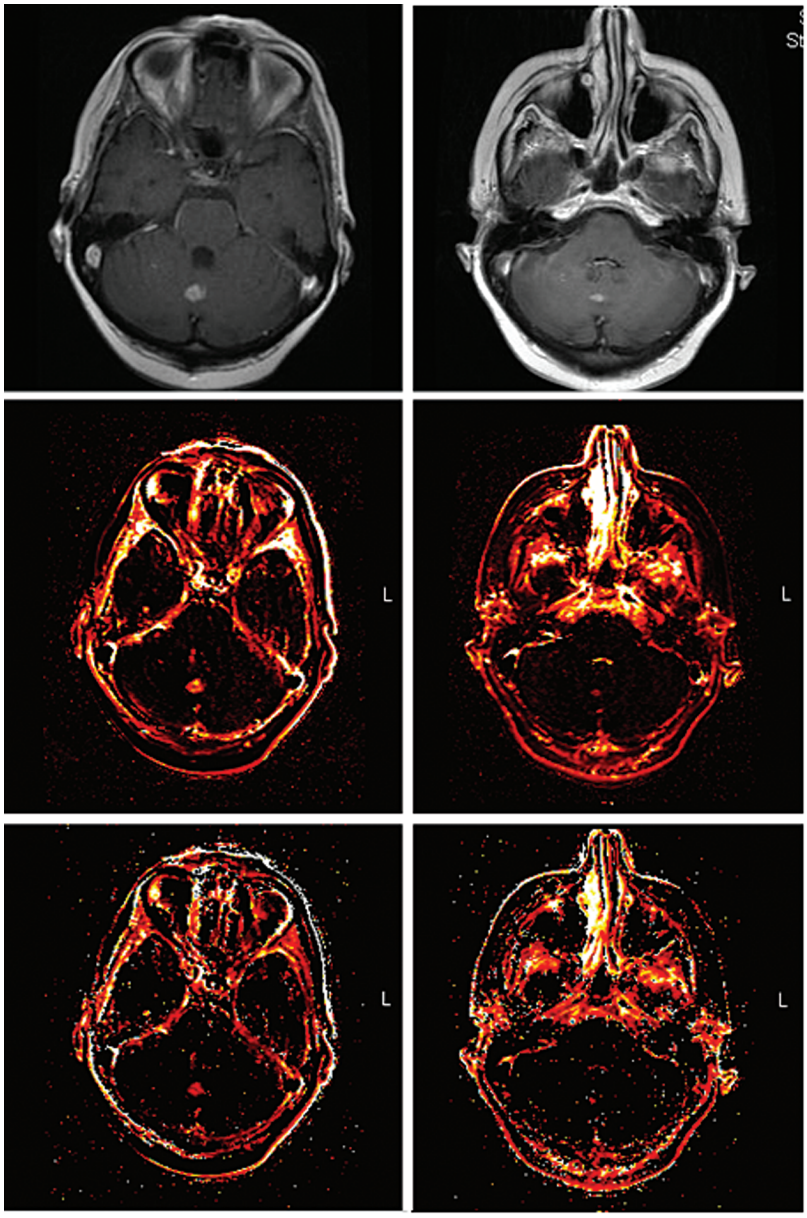

Fig. 2 From superior to inferior, images of T1-weighted postcontrast MRI, K^{trans}, and Ve before (left) and 8 weeks after (right) SRS to a midline cerebellar lesion. The post-RT K^{trans} SD was 0.0117 and this KRAS wild-type patient ultimately had an excellent partial response.

(n = 12) versus non-KRAS mutants (n = 21). The pre-RT Ve median for KRAS mutants was 30.25 and for the wild-type group 9.79. Using a Ve median cutoff value of 13.34, Ve was able to significantly predict KRAS mutant status compared with the Sequenom reference standard (area under the curve = 0.71, sensitivity = 81.8%, specificity = 61.9%).

Discussion

In this study, we evaluated MR perfusion imaging data to predict whether or not lung cancer BMs will ultimately respond or fail SRS treatment. Functional pMRI features outperformed early clinical assessment of conventional anatomic MRI using only size measurements. Our data show that post-RT K^{trans} SD within 12 weeks of SRS may be used as an imaging biomarker to predict long-term treatment response for lung cancer BMs. We were able to determine a post-RT K^{trans} SD cutoff value with nearly 90% sensitivity for early detection of nonresponders to treatment. Our findings may allow patients with NSCLC brain metastases suitable for SRS who undergo pretreatment pMRI and early posttreatment pMRI to be stratified by physiologic treatment response. Early identification of nonresponders can allow for timelier management decisions and potential avoidance of delayed salvage therapy

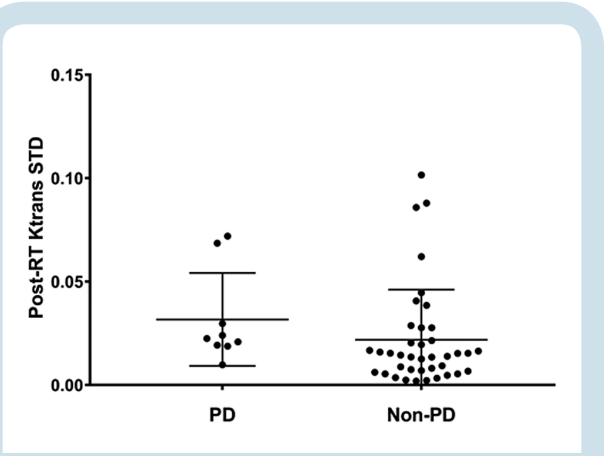

Fig. 3 Patients with PD showed significantly increased post-RT K^{trans} SD within 12 weeks of SRS compared with patients with nonprogressive disease (non-PD).

when chances of successful treatment are diminished. Several possible approaches for brain metastases that are likely to fail initial SRS (as determined by DCE-MRI) include RT intensification with repeat SRS, surgical resection, and laser ablation.[17–19] In addition to determining the utility of K^{trans} SD to identify potential nonresponders, we determined that Ve from pMRI can identify KRAS mutation status with >80% sensitivity.

K^{trans} derived from pMRI reflects the volume transfer constant of gadolinium from the intravascular compartment to the extracellular extravascular space and is partly dependent on vascular permeability. Human solid tumors display extensive variation in microvasculature, and therefore measuring the level of vascular heterogeneity within tumors can be an important tool for understanding tumor biology and predicting treatment outcome. K^{trans} SD is considered a noninvasive indicator of tumor vascular heterogeneity and has shown promise as a tumor imaging biomarker.[20,21] Jansen et al studied 12 patients with nodal metastases of head and neck cancer who ultimately underwent surgery.[22] They utilized DCE pMRI prior to treatment and correlated imaging findings to molecular studies. There was a significant negative correlation found between K^{trans} SD and Ki-67, which is a marker of cellular proliferation. This indicates that the proliferation of tumor cells is inversely correlated with tumor heterogeneity. Several studies have also demonstrated that pMRI biomarkers of tumor heterogeneity, including K^{trans} skewness and SD, correlate with overall survival, tumor grade, or RT outcome.[23–25]

Radiation therapy, particularly SRS, has well-established effects on tissue vasculature, including disruption of small vessels and causing early and durable endothelial damage.[26–29] BMs that failed SRS in our study demonstrated higher post-SRS K^{trans} SD and therefore probably increased tumor heterogeneity compared with successfully treated BMs. The increased heterogeneity might be attributable to areas of lower tumor proliferation and hypoxia in the PD group versus the non-PD group. Our findings agree with a breast cancer study that demonstrated an early posttreatment shift in pMRI heterogeneity biomarkers from heterogeneous to more homogeneous within tumors that responded favorably to treatment.[25] Another study, in rectal cancer patients, demonstrated a significant RT-related decrease in tumor vessel heterogeneity measured by pMRI.[24]

Ours is the first study to identify K^{trans} SD as a predictive biomarker for BM treatment outcome after SRS. Other studies have demonstrated the value of K^{trans} summary statistics, such as mean and/or median K^{trans}, in predicting treatment outcome after SRS. For example, Almeida-Freitas et al studied a mixed-histology cohort of 26 patients with 34 BMs treated with SRS.[30] All patients were treated with SRS and then reimaged 4–8 weeks after therapy. The researchers found that an increase of 15% in K^{trans} after SRS was significantly predictive of tumor progression. Jakubovic et al studied 70 histologically diverse BMs in 44 patients who received either SRS or WBRT.[31] Patients were imaged prior to treatment, 1 week after treatment, and again 1 month after treatment. The researchers found that lower K^{trans} median at 1 week posttreatment significantly discriminated responders from nonresponders. Our data also demonstrated lower K^{trans} median values for the non-PD group versus the PD group within 12 weeks after therapy. The difference in post-RT K^{trans} median between the PD group and non-PD group in our study demonstrated a trend toward statistical significance ($P = 0.55$).

Unlike the vast majority of prior studies evaluating BMs after RT, ours focused exclusively on NSCLC lesions treated with single modality SRS. This allows for control of potentially confounding variables such as variable tumor histologies and the effect of non-ablative radiation treatments such as whole brain radiation before SRS. We believe that another strength of our study is that the majority of patients were followed until death, giving us a more complete understanding of the long-term utility of pMRI biomarkers.

We additionally performed an exploratory analysis of perfusion imaging biomarkers correlated to molecular aberrations commonly found in NSCLC. We found that Ve may identify patients harboring a KRAS mutation with sensitivity greater than 80%. This study lends credence in allowing functional MRI techniques such as pMRI to evolve into a platform for personalization of therapy or even determination of risk factors. For example, KRAS G12C mutations are associated with previous tobacco exposure in NSCLC and are less often found in former and never smokers.[32,33] KRAS mutations are generally not yet considered actionable, but there is a renewed focus on personalizing therapy with either direct or indirect inhibition of this pathway.[34] There is limited, but growing, data correlating pMRI biomarkers with mutational status. Yeo et al studied 46 patients with pathologically confirmed rectal cancer who underwent DCE-MRI prior to surgery. There was an association of elevated K^{trans} mean with KRAS mutations that approached significance ($P = 0.060$). There was no association of Ve with KRAS mutations.[35]

Aside from its retrospective nature, our study had additional limitations. Our results cannot be generalized for a broad spectrum of tumor histologies because we focused on patients with NSCLC. BMs arising from NSCLC represent one of the most common types of BMs (along with

Table 2 Univariate analysis using Wilcoxon rank-sum test

Variable		With-PD Group Imaging Metric Values	Without-PD Group Imaging Metric Values	*P*
Pre-RT K^{trans}	Mean (range)	0.054 (0.005–0.079)	0.102 (0.008–0.474)	0.712
	SD (range)	0.023 (0.003–0.045)	0.052 (0.008–0.221)	0.328
	Median (range)	0.047 (0–0.090)	0.098 (0–0.540)	0.435
Pre-RT Ve	Mean (range)	21.7 (4.3–48.5)	28.3 (1.5–61.0)	0.373
	SD (range)	16.2 (3.6–50.9)	25.0 (3.5–84.0)	0.899
	Median (range)	19.3 (5.8–35.7)	24.3 (0–86)	0.228
Pre-RT Vp	Mean (range)	3.8 (0.5–9.7)	8.0 (0.2–57.9)	0.634
	SD (range)	1.7 (0.2–3.9)	4.3 (0.3–33.3)	0.303
	Median (range)	3.8 (0.4–10.7)	8.2 (0–62.4)	0.812
Post-RT K^{trans}	Mean (range)	0.057 (0.026–0.119)	0.044 (0.004–0.452)	0.064
	SD (range)	0.032 (0.010–0.072)	0.022 (0.002–0.135)	**0.032**
	Median (range)	0.055 (0.020–0.10)	0.038 (0–0.310)	0.055
Post-RT Ve	Mean (range)	23.7 (7.2–71.4)	15.6 (0.5–63.7)	0.064
	SD (range)	30.2 (4.3–40.0)	18.1 (17.9–94.5)	0.162
	Median (range)	12.1 (0–26.8)	11.3 (0–46.6)	0.236
Post-RT Vp	Mean (range)	1.6 (0.6–3.19)	1.8 (0.2–15.1)	0.526
	SD (range)	0.9 (0.1–1.7)	1.1 (0.1–6.6)	0.895
	Median (range)	1.4 (0–3.2)	1.8 (0–14.4)	0.833
Change in K^{trans}	Mean	0.003	−0.058	0.17
	SD	0.009	−0.030	0.054
	Median	0.008	−0.060	0.054
Change in Ve	Mean	2.0	−12.7	0.13
	SD	14.0	−6.9	0.17
	Median	−7.2	−13.0	0.42
Change in Vp	Mean	−2.2	−6.2	0.369
	SD	−0.8	−3.2	0.444
	Median	−2.4	−6.4	0.543
Clinical	Pre-RT volume, mm^3 (range)	1136.111 (125–2813)	852.821 (40–3960)	0.751
	Post-RT volume, mm^3 (range)	1523.611 (10–6075)	299.679 (0–2400)	0.405
	Mean total dose, Gy (range)	20.111 (18–21)	20.103(18–21)	0.754

Abbreviations: K^{trans}, time-dependent leakage; PD, progressive disease; Ve, extracellular extravascular volume; Vp = blood plasma volume.

breast cancer and melanoma) and those for which some of the greatest advances in targeted therapy have been made in the past decade.[36,37] Accurate prediction of failure of SRS can allow these patients to receive additional therapy earlier in their treatment course. Another limitation is that we do not have pathologic evidence that K^{trans} SD represents tumor heterogeneity because neurosurgical intervention was not feasible or practical in this patient population with stage IV disease. Our study may have also been potentially limited by inclusion of 5 BMs that were between 5 mm and 9 mm in size. We believe this was warranted, since many lesions less than 10 mm are routinely treated with SRS at our institution and others. Furthermore, we routinely image our SRS patients with high resolution T1-weighted contrast enhancement at 1 mm slice thickness and no interslice gap, thereby increasing confidence in the recorded measurements. Finally, we report our institutional protocol for capturing perfusion data, but these protocols vary among institutions, further limiting applicability until consensus protocols can be determined.

In conclusion, this study demonstrates promising evidence that pMRI biomarkers measured within 12 weeks after SRS for NSCLC BMs can be used to predict long-term local control and outperform early assessment of simple anatomic changes measured by conventional MRI. Perfusion imaging biomarkers may also have utility in determining the presence or absence of molecular aberrations. These findings can potentially help guide and personalize patient treatment decisions. Larger studies are required to prospectively validate our results.

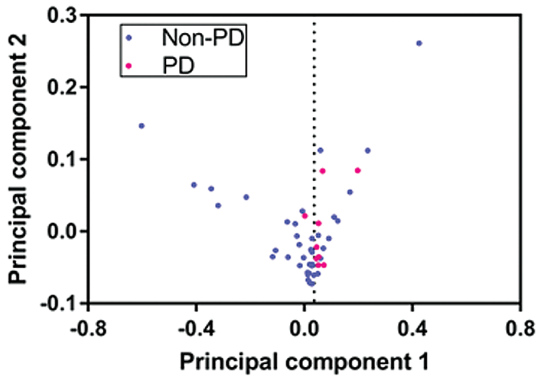

Fig. 4 Scatter plot of patients with and without PD after principal component analysis using 5 features with $P < 0.1$ in a univariate Wilcoxon rank-sum test.

Funding

This work was supported by the National Institutes of Health/ National Cancer Institute (Cancer Center Support Grant P30 CA008748).

Acknowledgment

The authors thank Joanne Chin, who provided editorial support.

Conflict of interest statement. None.

References

1. Barnholtz-Sloan JS, Sloan AE, Davis FG, Vigneau FD, Lai P, Sawaya RE. Incidence proportions of brain metastases in patients diagnosed (1973 to 2001) in the Metropolitan Detroit Cancer Surveillance System. *J Clin Oncol*. 2004;22(14):2865–2872.
2. Patchell RA. The management of brain metastases. *Cancer Treat Rev*. 2003;29(6):533–540.
3. Sperduto PW, Kased N, Roberge D, et al. Summary report on the graded prognostic assessment: an accurate and facile diagnosis-specific tool to estimate survival for patients with brain metastases. *J Clin Oncol*. 2012;30(4):419–425.
4. Moraes FY, Taunk NK, Marta GN, Suh JH, Yamada Y. The rationale for targeted therapies and stereotactic radiosurgery in the treatment of brain metastases. *Oncologist*. 2016;21(2):244–251.
5. Goyal S, Silk AW, Tian S, et al. Clinical management of multiple melanoma brain metastases: a systematic review. *JAMA Oncol*. 2015;1(5):668–676.
6. Mehta MP, Tsao MN, Whelan TJ, et al. The American Society for Therapeutic Radiology and Oncology (ASTRO) evidence-based review of the role of radiosurgery for brain metastases. *Int J Radiat Oncol Biol Phys*. 2005;63(1):37–46.
7. Aoyama H, Shirato H, Tago M, et al. Stereotactic radiosurgery plus whole-brain radiation therapy vs stereotactic radiosurgery alone for treatment of brain metastases: a randomized controlled trial. *JAMA*. 2006;295(21):2483–2491.
8. Fink KR, Fink JR. Imaging of brain metastases. *Surg Neurol Int*. 2013;4(Suppl 4):S209–S219.
9. Nowosielski M, Radbruch A. The emerging role of advanced neuroimaging techniques for brain metastases. *Chin Clin Oncol*. 2015;4(2):23.
10. Jackson A, O'Connor J, Thompson G, Mills S. Magnetic resonance perfusion imaging in neuro-oncology. *Cancer Imaging*. 2008;8:186–199.
11. Patel TR, McHugh BJ, Bi WL, Minja FJ, Knisely JP, Chiang VL. A comprehensive review of MR imaging changes following radiosurgery to 500 brain metastases. *AJNR Am J Neuroradiol*. 2011;32(10):1885–1892.
12. Lin NU, Lee EQ, Aoyama H, et al; Response Assessment in Neuro-Oncology (RANO) group. Response assessment criteria for brain metastases: proposal from the RANO group. *Lancet Oncol*. 2015;16(6):e270–e278.
13. Kohutek ZA, Yamada Y, Chan TA, et al. Long-term risk of radionecrosis and imaging changes after stereotactic radiosurgery for brain metastases. *J Neurooncol*. 2015;125(1):149–156.
14. Kadota K, Sima CS, Arcila ME, et al. KRAS mutation is a significant prognostic factor in early-stage lung adenocarcinoma. *Am J Surg Pathol*. 2016;40(12):1579–1590.
15. Tofts PS. Modeling tracer kinetics in dynamic Gd-DTPA MR imaging. *J Magn Reson Imaging*. 1997;7(1):91–101.
16. Tofts PS, Brix G, Buckley DL, et al. Estimating kinetic parameters from dynamic contrast-enhanced T(1)-weighted MRI of a diffusable tracer: standardized quantities and symbols. *J Magn Reson Imaging*. 1999;10(3):223–232.
17. McKay WH, McTyre ER, Okoukoni C, et al. Repeat stereotactic radiosurgery as salvage therapy for locally recurrent brain metastases previously treated with radiosurgery. *J Neurosurg*. 2017;127(1):148–156.
18. Rao MS, Hargreaves EL, Khan AJ, Haffty BG, Danish SF. Magnetic resonance-guided laser ablation improves local control for postradiosurgery recurrence and/or radiation necrosis. *Neurosurgery*. 2014;74(6):658–667; discussion 667.
19. Koffer P, Chan J, Rava P, et al. Repeat stereotactic radiosurgery for locally recurrent brain metastases. *World Neurosurg*. 2017;104:589–593.
20. Jackson A, O'Connor JP, Parker GJ, Jayson GC. Imaging tumor vascular heterogeneity and angiogenesis using dynamic contrast-enhanced magnetic resonance imaging. *Clin Cancer Res*. 2007;13(12):3449–3459.
21. Lee CH, Choi JW, Kim KA, Seo TS, Lee JM, Park CM. Usefulness of standard deviation on the histogram of ultrasound as a quantitative value for hepatic parenchymal echo texture; preliminary study. *Ultrasound Med Biol*. 2006;32(12):1817–1826.
22. Jansen JF, Carlson DL, Lu Y, et al. Correlation of a priori DCE-MRI and (1) H-MRS data with molecular markers in neck nodal metastases: initial analysis. *Oral Oncol*. 2012;48(8):717–722.
23. Shukla-Dave A, Lee NY, Jansen JF, et al. Dynamic contrast-enhanced magnetic resonance imaging as a predictor of outcome in head-and-neck squamous cell carcinoma patients with nodal metastases. *Int J Radiat Oncol Biol Phys*. 2012;82(5):1837–1844.
24. de Lussanet QG, Backes WH, Griffioen AW, et al. Dynamic contrast-enhanced magnetic resonance imaging of radiation therapy-induced microcirculation changes in rectal cancer. *Int J Radiat Oncol Biol Phys*. 2005;63(5):1309–1315.

25. Issa B, Buckley DL, Turnbull LW. Heterogeneity analysis of Gd-DTPA uptake: improvement in breast lesion differentiation. *J Comput Assist Tomogr*. 1999;23(4):615–621.
26. O'Connor MM, Mayberg MR. Effects of radiation on cerebral vasculature: a review. *Neurosurgery*. 2000;46(1):138–149; discussion 150–151.
27. Lucas J, Mack WJ. Effects of ionizing radiation on cerebral vasculature. *World Neurosurg*. 2014;81(3-4):490–491.
28. Brown JM, Carlson DJ, Brenner DJ. The tumor radiobiology of SRS and SBRT: are more than the 5 Rs involved? *Int J Radiat Oncol Biol Phys*. 2014;88(2):254–262.
29. Song CW, Kim MS, Cho LC, Dusenbery K, Sperduto PW. Radiobiological basis of SBRT and SRS. *Int J Clin Oncol*. 2014;19(4):570–578.
30. Almeida-Freitas DB, Pinho MC, Otaduy MC, Braga HF, Meira-Freitas D, da Costa Leite C. Assessment of irradiated brain metastases using dynamic contrast-enhanced magnetic resonance imaging. *Neuroradiology*. 2014;56(6):437–443.
31. Jakubovic R, Sahgal A, Soliman H, et al. Magnetic resonance imaging-based tumour perfusion parameters are biomarkers predicting response after radiation to brain metastases. *Clin Oncol (R Coll Radiol)*. 2014;26(11):704–712.
32. Seo KY, Jelinsky SA, Loechler EL. Factors that influence the mutagenic patterns of DNA adducts from chemical carcinogens. *Mutat Res*. 2000;463(3):215–246.
33. Prior IA, Lewis PD, Mattos C. A comprehensive survey of Ras mutations in cancer. *Cancer Res*. 2012;72(10):2457–2467.
34. McCormick F. KRAS as a therapeutic target. *Clin Cancer Res*. 2015;21(8):1797–1801.
35. Yeo DM, Oh SN, Jung CK, et al. Correlation of dynamic contrast-enhanced MRI perfusion parameters with angiogenesis and biologic aggressiveness of rectal cancer: preliminary results. *J Magn Reson Imaging*. 2015;41(2):474–480.
36. Owonikoko TK, Arbiser J, Zelnak A, et al. Current approaches to the treatment of metastatic brain tumours. *Nat Rev Clin Oncol*. 2014;11(4):203–222.
37. Grommes C, Oxnard GR, Kris MG, et al. "Pulsatile" high-dose weekly erlotinib for CNS metastases from EGFR mutant non-small cell lung cancer. *Neuro Oncol*. 2011;13(12):1364–1369.